

CHEMISTRY

Low-temperature gas-phase formation of indene in the interstellar medium

Srinivas Doddipatla¹, Galiya R. Galimova^{2,3}, Hongji Wei⁴, Aaron M. Thomas¹, Chao He¹, Zhenghai Yang¹, Alexander N. Morozov², Christopher N. Shingledecker^{4*}, Alexander M. Mebel^{2*}, Ralf I. Kaiser^{1*}

Polycyclic aromatic hydrocarbons (PAHs) are fundamental molecular building blocks of fullerenes and carbonaceous nanostructures in the interstellar medium and in combustion systems. However, an understanding of the formation of aromatic molecules carrying five-membered rings—the essential building block of nonplanar PAHs—is still in its infancy. Exploiting crossed molecular beam experiments augmented by electronic structure calculations and astrochemical modeling, we reveal an unusual pathway leading to the formation of indene (C₉H₈)—the prototype aromatic molecule with a five-membered ring—via a barrierless bimolecular reaction involving the simplest organic radical—methylidyne (CH)—and styrene (C₆H₅C₂H₃) through the hitherto elusive methylidyne addition–cyclization–aromatization (MACA) mechanism. Through extensive structural reorganization of the carbon backbone, the incorporation of a five-membered ring may eventually lead to three-dimensional PAHs such as corannulene (C₂₀H₁₀) along with fullerenes (C₆₀, C₇₀), thus offering a new concept on the low-temperature chemistry of carbon in our galaxy.

INTRODUCTION

Since Léger's and Puget's very first hypothesis of polycyclic aromatic hydrocarbons (PAHs)—organic molecules composed of fused benzene rings—as the missing link between small carbon molecules and carbonaceous nanoparticles (interstellar grains) (1), PAHs (2) along with their (de)hydrogenated (3), alkylated (4, 5), protonated (6), and ionized (7) counterparts have been associated with the diffuse interstellar bands (DIBs) (8)—discrete absorption features superimposed on the interstellar extinction curve ranging from the visible (400 nm) to the near-infrared (1.2 μm)—and the unidentified infrared (UIR) emission bands (9, 10) in the 3- to 14-μm range. Encompassing up to 20% of the carbon budget in our galaxy (11, 12), the identification of PAHs in carbonaceous chondrites such as Murchison, Allende, and Orgueil (13, 14) along with ¹³C/¹²C and D/H isotopic analyses (15) advocates a circumstellar origin of aromatics in carbon-rich asymptotic giant branch (AGB) stars and planetary nebulae as the descendants of AGB stars at elevated temperatures of a few 1000 K through molecular mass growth processes involving hydrogen abstraction–carbon addition (HACA) sequences (16).

Micelotta *et al.* (17, 18) revealed that, once formed, interstellar PAHs are swiftly destroyed by galactic cosmic rays, photolysis, and shock waves, causing lifetimes of only a few 10⁸ years. These time scales are substantially shorter than those for the injection of PAHs from carbon-rich circumstellar envelopes into the interstellar medium of 2 × 10⁹ years (19–22). Consequently, PAHs should exist neither in the interstellar medium nor in meteorites, and the ubiquitous presence of PAHs represents a key paradox in astrophysics. This inconsistency could be resolved by inferring the existence of hitherto elusive low-temperature routes to a rapid growth of PAHs in the in-

terstellar medium to offset their destruction (23). An identification of these low-temperature pathways is of particular importance to untangle the origin of PAHs carrying five-membered rings such as indene, which represents an essential molecular building block of nonplanar PAHs like corannulene (Fig. 1). Nonplanar PAHs—potential precursors to fullerenes (24, 25)—require five-membered rings in the carbon backbone to bend PAHs out of the plane and to ultimately form three-dimensional carbonaceous nanostructures (26). However, the low-temperature formation mechanisms of even the simplest prototype of a PAH carrying a five-membered ring—indene (C₉H₈)—from astrochemically relevant precursor molecules are still unknown. This requires an intimate understanding of the elementary reactions and dynamics of reactions leading to indene on the most fundamental, microscopic level (27).

Here, we reveal that the indene molecule (C₉H₈) can be synthesized barrierlessly via the elementary reaction of the simplest organic radical—methylidyne (CH)—with styrene (C₆H₅ C₂H₃) under single collision conditions. Combining crossed molecular beam reactive scattering experiments with electronic structure calculations and astrochemical modeling, our study implicates an unexpected gas-phase chemistry initiated by a single collision event, which operates even at temperature as low as 10 K present in cold molecular clouds like the Taurus Molecular Cloud (TMC-1) and the Orion Molecular Cloud. The reaction of methylidyne with styrene involves a hitherto elusive low-temperature methylidyne addition–cyclization–aromatization (MACA) mechanism and may exemplify the prototype of a barrierless pathway to indene in those molecular clouds, where a rapid gas-phase chemistry follows ice mantle sublimation. MACA operates at ultralow temperatures and eventually transforms a vinyl (C₂H₃) side group of aromatic molecules to a fused pentacycle involving an extensive reorganization of the carbon skeleton. These findings dispute established paradigms that molecular mass growth processes to nonplanar PAHs operate only at high temperatures such as in circumstellar envelopes of carbon stars and in combustion systems (28) and suggest that a low-temperature chemistry can initiate the formation of the very first aromatic molecules in the interstellar

Copyright © 2021
The Authors, some
rights reserved;
exclusive licensee
American Association
for the Advancement
of Science. No claim to
original U.S. Government
Works. Distributed
under a Creative
Commons Attribution
NonCommercial
License 4.0 (CC BY-NC).

¹Department of Chemistry, University of Hawai'i at Mānoa, Honolulu, HI 96822, USA. ²Department of Chemistry and Biochemistry, Florida International University, Miami, FL, 33199, USA. ³Samara National Research University, Samara 443086, Russia. ⁴Department of Physics and Astronomy, Benedictine College, Atchison, KS 66002, USA.

*Corresponding author. Email: ralfk@hawaii.edu (R.I.K.); mebel@fiu.edu (A.M.M.); cshingledecker@benedictine.edu (C.N.S.)

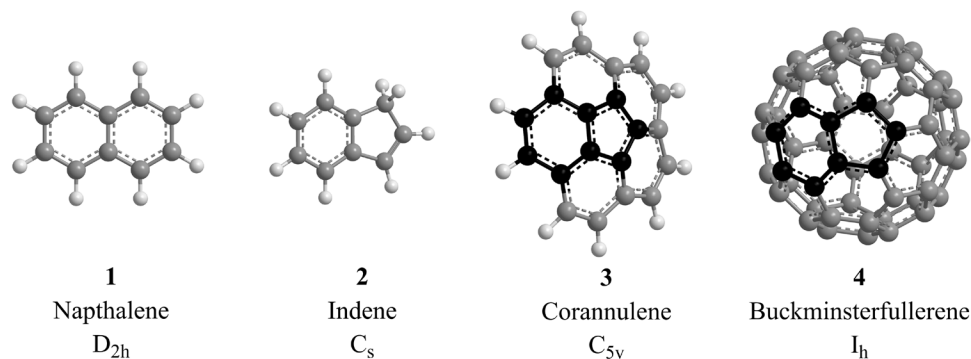


Fig. 1. Simplest representatives of two-ring PAHs carrying two six-membered (naphthalene, $C_{10}H_8$; **1) and one six- along with one five-membered ring (indene, C_9H_8 ; **2**).** Whereas the hydrogen abstraction–vinylacetylene addition (HAVA) mechanism can lead to the formation of naphthalene at 10 K, a low-temperature pathway to indene—a fundamental molecular building block of bent PAHs like corannulene ($C_{20}H_{10}$; **3**) and buckminsterfullerene (C_{60} ; **4**)—is still elusive. Carbon and hydrogen atoms are color-coded in gray and white, respectively, with the carbon backbone of indene highlighted in black.

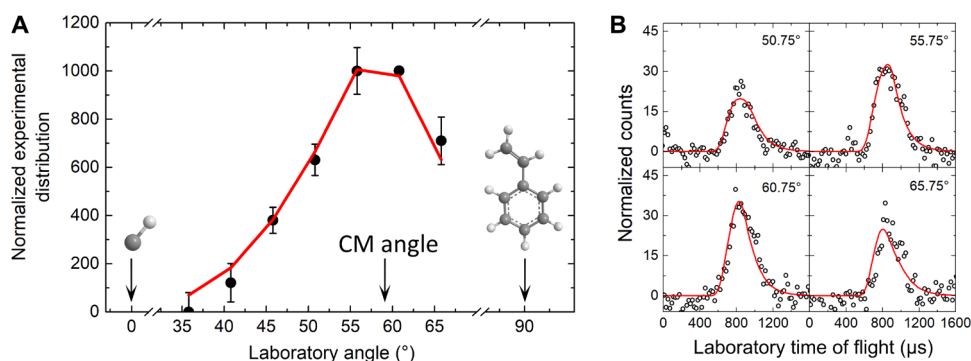


Fig. 2. Laboratory angular distribution and the associated time-of-flight spectra. Laboratory angular distribution at mass-to-charge ratio of 116 ($C_9H_8^+$) recorded in the reaction of the methylidyne radical (CH ; $X^2\Pi$) with styrene (C_8H_8 ; X^1A') (**A**) and the TOF spectra collected at distinct laboratory angles overlaid with the best fits (**B**). The solid circles with their error bars indicate the normalized experimental distribution with $\pm 1\sigma$ uncertainty, and the open circles indicate the experimental data points of the TOF spectra. The red lines represent the best fits obtained from the optimized center-of-mass (CM) functions, as depicted in Fig. 3.

medium carrying a five-membered ring: indene. The carbon backbone of indene—the simplest representative of an aromatic molecule carrying a six-membered benzene ring fused with a five-membered cyclopentadiene moiety—represents a fundamental molecular building block of nonplanar PAHs like corannulene ($C_{20}H_{10}$) and may signify an essential reaction intermediate in the molecular mass growth processes, leading ultimately to interstellar fullerenes (C_{60} , C_{70}) (24, 25).

RESULTS

Crossed molecular beam studies—Laboratory frame

The reactive scattering experiments were carried out exploiting a crossed molecular beam apparatus (Materials and Methods). For the reaction of the methylidyne radical [CH ; 13 atomic mass units (amu)] with styrene (C_8H_8 ; 104 amu), reactively scattered products were observed at mass/charge ratio (m/z) of 117 ($C_9H_9^+$), 116 ($C_9H_8^+$), and 115 ($C_9H_7^+$) with relative intensities of $10 \pm 2\%$, 100%, and $200 \pm 10\%$, respectively. The scattering signal was relatively weak; hence, at each angle, up to 5×10^6 time-of-flight (TOF) spectra had to be averaged over 50 hours to obtain reasonable signal-to-noise ratios. After scaling, the TOF spectra at all 3 m/z values were found to be superimposable. These findings propose that signal at $m/z = 116$ arises from the

hydrogen atom loss channel accompanied by the formation of a molecule with the molecular formula C_9H_8 formed via the reaction CH (13 amu) + C_8H_8 (104 amu) \rightarrow C_9H_8 (116 amu) + H (1 amu). Signal at $m/z = 117$ ($^{13}CC_8H_8^+$) arises from the natural abundance of ^{13}C isotope of carbon, whereas ion counts at $m/z = 115$ are connected to dissociative electron impact ionization of the neutral reaction products in the detector. Therefore, having evidenced the formation of molecule(s) with the formula C_9H_8 , TOF spectra of the nascent C_9H_8 reaction product were collected at $m/z = 116$ at distinct laboratory angles from 36° to 66° in 5° intervals. The TOFs were then normalized with respect to the TOF at the center of mass (Θ_{CM}) and integrated to yield the laboratory angular distribution (LAD) (Fig. 2). Notable features of the LAD of the C_9H_8 product(s) are the symmetry around the CM angle and the angular spread of at least 30° in the scattering plane, suggesting indirect scattering dynamics via the formation of C_9H_9 complexes.

Crossed molecular beam studies—CM frame

To unravel the underlying reaction mechanism(s) along with the nature of the C_9H_8 isomer(s), the experimental data were transformed from the laboratory to the CM reference frame (29, 30). This forward convolution approach yields the CM translational $P(E_T)$ and angular flux $T(\theta)$ distribution as depicted in Fig. 3. Best fits of the laboratory

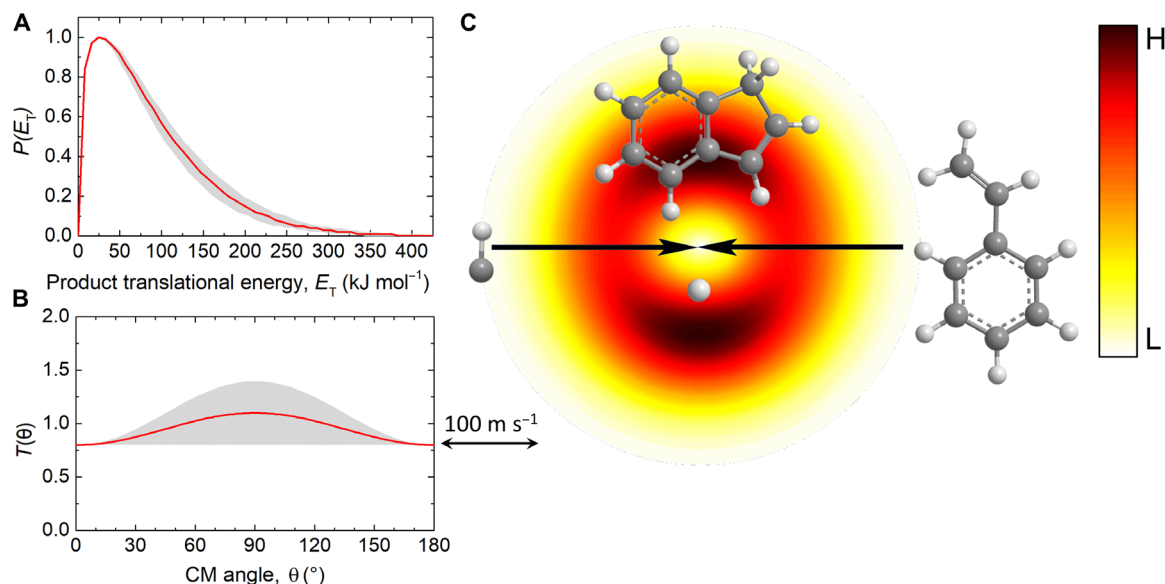


Fig. 3. CM distributions and the associated flux contour map. CM translational energy flux distribution (A), CM angular flux distribution (B), and the top view of the corresponding flux contour map (C) leading to the formation of indene plus atomic hydrogen in the reaction of methylidyne radical with styrene. Shaded areas indicate the error limits of the best fits accounting for the uncertainties of the laboratory angular distribution and TOF spectra, with the red solid lines defining the best-fit functions. The flux contour map represents the flux intensity of the reactive scattering products as a function of the CM scattering angle (θ) and product velocity (u). The color bar indicates the flux gradient from high (H) intensity to low (L) intensity. Atoms are color-coded in gray (carbon) and white (hydrogen).

data are accomplished with a single-channel fit forming products with a mass combination of 116 amu (C_9H_8) and 1 amu (H). A detailed inspection of the CM functions delivers critical information on the pertinent reaction channel(s) and dynamics. First, $P(E_T)$ assists in the identification of the product isomer(s). Accounting for the conservation of energy, for those products formed without internal excitation, the high-energy cutoff of 376 ± 38 kJ mol⁻¹ denotes the sum of the absolute value of the reaction exoergicity plus the collision energy E_C (20.6 ± 0.2 kJ mol⁻¹). The subtraction of the collision energy reveals that the reaction is highly exoergic by -355 ± 38 kJ mol⁻¹. This value agrees nicely with the National Institute of Standards and Technology (NIST) reaction energy of -364 ± 12 kJ mol⁻¹ to form the indene isomer along with atomic hydrogen (31). Furthermore, the $P(E_T)$ function holds a distribution maximum at 25 ± 3 kJ mol⁻¹, indicating a tight exit transition state. Last, the $T(\theta)$ distribution depicts flux over the complete angular range along with a forward-backward symmetry. This finding proposes indirect scattering dynamics via the formation of C_9H_9 complex(es) having a lifetime(s) longer than the (ir) rotational period. The pronounced distribution maximum at 90° suggests geometrical constraints of the decomposing complex(es), i.e., a preferential emission of the hydrogen atom in the exit transition state perpendicular to the rotational plane of the decomposing intermediate nearly parallel to the total angular momentum vector (32, 33).

Electronic structure calculations and formation mechanism

The present study reveals that at least the indene molecule—the prototype aromatic molecule carrying one five- and one six-membered ring—can be formed via the elementary reactions of the methylidyne radical with styrene in the gas phase. We are combining these findings with computational and statistical results to propose the underlying reaction mechanism(s) (Fig. 4 and fig. S1). The compu-

tations reveal that the methylidyne radical can add barrierlessly either to the π electron density of the carbon-carbon double bond of the vinyl moiety (C_2H_3) (Fig. 4A) or to the aromatic ring (Fig. 4, B and C). In analogy to the stem compounds ethylene (C_2H_4) (34) and benzene (C_6H_6) (35), methylidyne is unlikely to insert into any carbon-hydrogen bond of the phenyl or vinyl functional groups. The addition of methylidyne to the vinyl moiety leads to a phenyl-substituted cyclopropanyl intermediate (i1), which ring-opens to the thermodynamically preferred phenyl-substituted allylic radical intermediate (i2). The latter undergoes cis-trans isomerization to i3 followed by cyclization to i4; this reaction sequence is terminated by a hydrogen atom emission from the bridging C4 carbon atom accompanied by aromatization and formation of indene (p1) in an overall exoergic (-356 ± 8 kJ mol⁻¹) reaction through a tight exit transition state.

The addition of methylidyne to the benzene moiety is more complex because six chemically nonequivalent “aromatic” carbon-carbon bonds exist. The barrierless addition leading to intermediate i5, which undergoes a facile ring opening via a barrier of only 8 kJ mol⁻¹ to the vinyl-tropylyl radical intermediate i6, is exemplified in Fig. 4 (B and C). Note that the addition process to any aromatic carbon-carbon bond followed by ring opening results in the formation of the doublet radical intermediate i6 (fig. S2). This intermediate isomerizes via ring contraction to the bicyclic intermediate (i7) followed by the four-membered ring opening to an open-shell disubstituted cyclopentadiene derivative (i8). Three distinct reaction pathways lead ultimately to the 1*H*-inden-6-yl-1,5-dihydro intermediate (i11), which eventually fragments via a hydrogen atom loss from the CH_2 moiety located at the six-membered ring complemented by aromatization and synthesis of indene (p1) once again via a tight exit transition state. These isomerization sequences involve rotations of the side chains—one of them representing the vinyl side chain of the

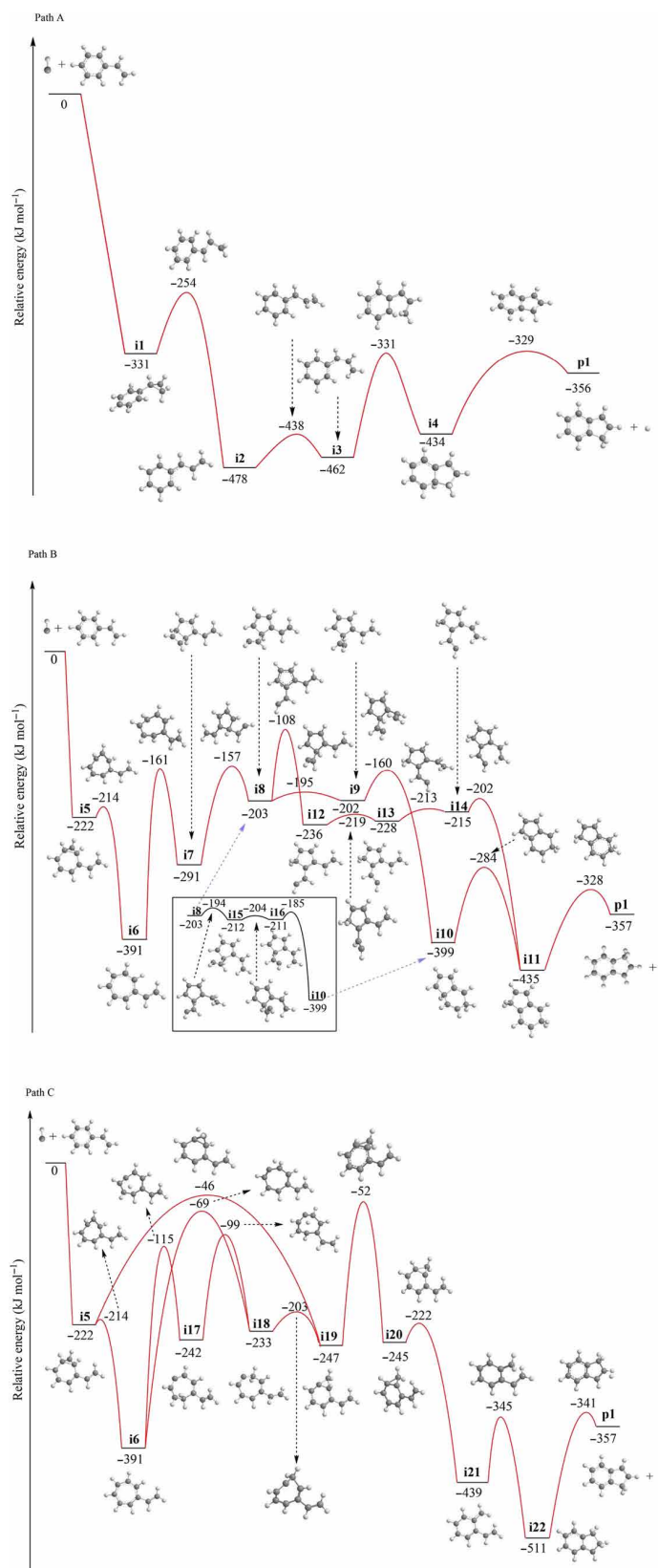


Fig. 4. Potential energy surface. The potential energy surface for the reaction of the methylidyne radical with styrene including reaction pathways energetically accessible in the crossed molecular beam experiments via addition to the vinyl (path A) and benzene moiety (paths B and C). The route in red highlights the reaction pathway leading to the formation of indene plus atomic hydrogen. Relative energies are given in units of kJ mol⁻¹. Atoms are color-coded in gray (carbon) and white (hydrogen).

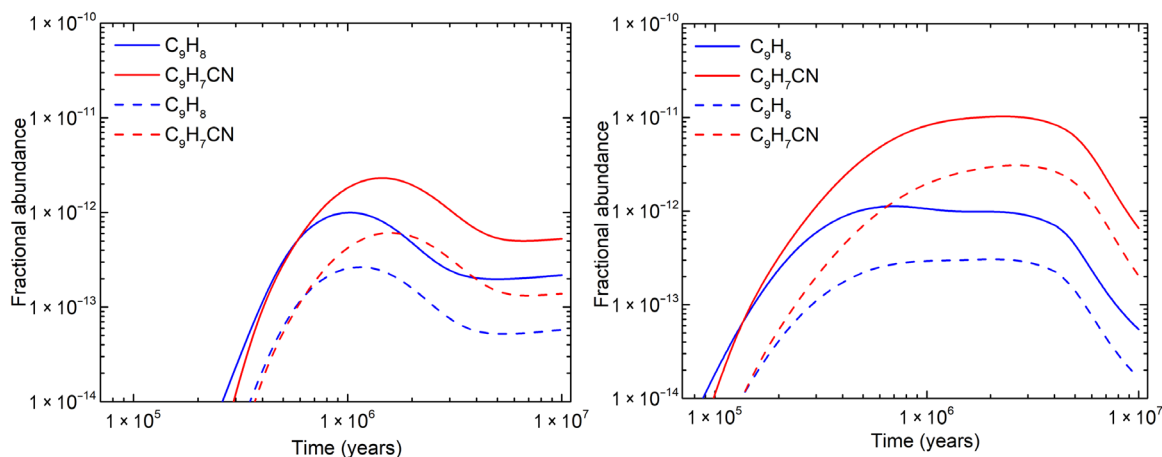


Fig. 5. Modeled fractional abundances of indene (C_9H_8) and cyanoindene (C_9H_7CN) in cold molecular clouds. (Left) Simulation with a cosmic ray ionization rate of $\zeta = 1.3 \times 10^{-17} \text{ s}^{-1}$. (Right) Simulation with a cosmic ray ionization rate of $\zeta = 1.3 \times 10^{-16} \text{ s}^{-1}$. The solid and dashed lines depict upper and lower limits of the fractional abundances (Supplementary Materials).

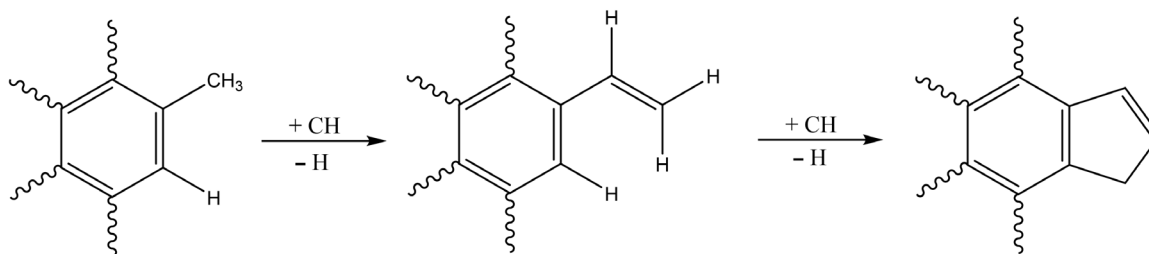


Fig. 6. Versatile conversion of a methyl (CH_3) functional group of a PAH to the indene moiety via methylidyne radical reactions through vinyl (C_2H_3) substituted PAHs involving the novel methylidyne addition–cyclization–aromatization (MACA) mechanism. The waved lines indicate the incorporation within a PAH.

styrene reactant—around the C—C bonds connecting them with the five-membered ring (**i8** → **i9**, **i8** → **i15** → **i16**, or **i12** → **i13** → **i14**), which may be preceded by hydrogen migration in the five-membered ring (**i8** → **i12**). The rotations are followed by ring closures (**i9** → **i10** or **i14** → **i11**), in which the six-membered ring is reformed from two exocyclic C2 moieties; the bicyclic intermediate **i10** is linked to **i11** via H migration in the five-membered ring. Alternatively, intermediate **i6** could isomerize in one or two steps involving (multiple) hydrogen migration steps leading to **i18**, followed by a sequence of ring contraction (**i19**) – hydrogen shift (**i20**) – ring opening (**i21**) – and cyclization (**i22**). The 1-indanyl radical represents the global minimum of the C_9H_9 potential energy surface and undergoes unimolecular decomposition via a loss of atomic hydrogen from the methylidyne moiety at the C2 carbon through a tight exit transition state accompanied by aromatization and formation of indene (**p1**).

Having identified six feasible reaction pathways leading eventually to indene plus atomic hydrogen, we are exploiting now a Rice-Ramsperger-Kassel-Marcus (RRKM) master equation analysis (Materials and Methods) to predict the dominating reaction pathway(s) to indene. First, we evaluate the probability of methylidyne addition to the C=C double bond in the vinyl side chain versus the addition to the benzene ring. The rate constant for methylidyne addition to the double bond in the side chain is expected to be close to that for the prototype methylidyne-ethylene reaction, which, according to the literature data, is in the range of 3×10^{-10} to $5 \times 10^{-10} \text{ cm}^3 \text{ molecule}^{-1} \text{ s}^{-1}$ for 23

to 300 K (36, 37) and 2×10^{-10} to $3 \times 10^{-10} \text{ cm}^3 \text{ molecule}^{-1} \text{ s}^{-1}$ for 300 to 700 K (38). While for the methylidyne-benzene system experimental kinetic data are available for 25 K ($2.7 \times 10^{-10} \text{ cm}^3 \text{ molecule}^{-1} \text{ s}^{-1}$) (39) and from 297 to 674 K (40) with nearly temperature-independent rates of $4 \times 10^{-10} \text{ cm}^3 \text{ molecule}^{-1} \text{ s}^{-1}$ (36), our present variable reaction coordinate transition state theory (VRC-TST) calculations of methylidyne addition to the aromatic ring in benzene and to the double C=C bond in ethylene revealed that the rate constants for the former are by a factor of typically 1.5 higher than those for the latter in the same temperature interval (Supplementary Materials). The temperature dependence of the calculated rate constant for methylidyne-benzene is similar to that for the experimental rate constant for methylidyne-ethylene, and the computed values for both reactions reproduce the experimental measurements within 20% or better. On the basis of this comparison, we can anticipate that methylidyne addition to the benzene ring should be approximately 1.5 times more likely than methylidyne addition to the vinyl side chain. Next, according to RRKM calculations of product branching ratios at the experimental collision energy, the addition to the side chain nearly exclusively produces indene via hydrogen atom loss from the benzene ring ($96 \pm 2\%$ versus $4 \pm 2\%$; **p2**). Alternatively, methylidyne addition to the benzene ring is predicted to result in the production of $63 \pm 6\%$ indene (by hydrogen atom loss from the vinyl chain), $33 \pm 6\%$ vinylcyclopentadienyl plus acetylene (**p5**), and $5 \pm 3\%$ other C_9H_8 isomers with the indene core (**p3** and **p4**; fig. S1), which might be formed

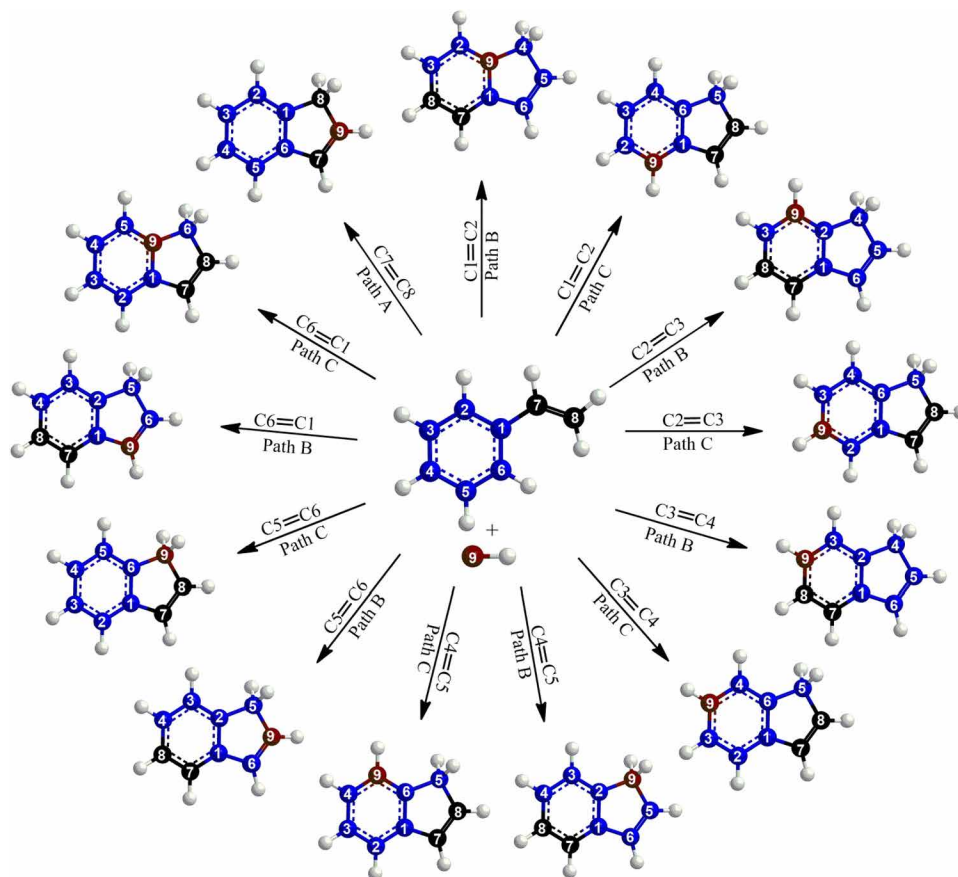


Fig. 7. Indene carbon skeleton. Location of the carbon atoms within the styrene and methylidyne reactants and for the indene reaction product following addition to the vinyl (path A) and benzene moieties (paths B and C).

via hydrogen atom losses from both the ring and the vinyl chain. Note that the error bars in the computed branching ratios were assessed by varying the heights of the critical barriers for different product channels by ± 4 kJ mol⁻¹, which is the typical expected accuracy for relative energies computed in this study. Neglecting the small contribution from the alternative C₉H₈ isomers **p3** and **p4**, we evaluate the relative yields of hydrogen atom losses from the side chain and the benzene ring as $1.5 \times 0.63/1$ or nearly 1:1. Thus, the pathways to indene initiating with methylidyne addition to the ring, predominantly via intermediates **i6**, **i7**, **i8**, and **i11**, are as likely as the **i1** → **i2** → **i3** → **i4** → **p1** route initiating with methylidyne addition to the side chain. According to the predicted reaction mechanism, indene cannot be formed by elimination of the hydrogen atom originating from the methylidyne reactant.

Astrochemical modeling

Having provided compelling evidence on the formation of indene under single collision conditions via the MACA mechanism, we are examining through astrochemical modeling how these findings can be transferred from the laboratory to the interstellar medium. This is central because crossed molecular beam experiments along with computations cannot simulate the chemical complexity in molecular clouds. The computations predict that the elementary reaction of methylidyne with styrene has no entrance barrier to addition, all barriers implicated in the formation of indene are situated below the energy of the separated reactants, and the overall reaction to indene

is exoergic. These findings signify vital criteria for this reaction to be open in low-temperature environments such as in molecular clouds, which have temperatures as low as 10 K. Any barrier would block these reactions in low-temperature interstellar environments. Therefore, our results can be applied to any cold environment in deep space such as molecular clouds, where both the methylidyne and styrene reactants exist. Methylidyne radicals can be generated in the gas-phase photolysis of methane (CH₄) (41) by Lyman α even present within the internal ultraviolet (UV) photon field deep inside molecular clouds (42). Styrene can be formed either via the barrierless, bimolecular reaction of a methylidyne radical with toluene (C₆H₅CH₃) [fig. S3 (43)] or via UV- and galactic cosmic ray-induced (reactive) desorption along with grain-grain collisions and removal of ice mantles of grains containing styrene (44, 45). Toluene itself can be produced barrierlessly from acyclic species in bimolecular ethynyl (C₂H) plus isoprene (C₅H₈) (46) and 1-propynyl (CH₃CC) plus 1,3-butadiene (C₄H₆) (47) reactions. To explore the overall efficiency of MACA on the formation of indene in the interstellar medium, astrochemical simulations were run for the cold molecular cloud TMC-1 using the Nautilus v1.1 code (48). Most of the physical parameters and initial fractional abundances of the reactive species were adopted from Hincelin *et al.* (49) and are described in more detail in the Supplementary Materials. This reaction network was updated to include chemistries leading eventually to the indene molecule as elucidated in the present work.

These modeling studies reveal exciting findings (Fig. 5). The left-hand panel shows the results of the simulation with the standard cosmic ray ionization rate of $\zeta = 1.3 \times 10^{-17} \text{ s}^{-1}$, while the right-hand panel depicts results using a value of $\zeta = 1.3 \times 10^{-16} \text{ s}^{-1}$, which is in line with data recently derived by Ivlev *et al.* (50) for L1544, another source in Taurus. The astrochemical models disclose significant amounts of indene formed via MACA in the gas phase at fractional abundances of up to a few 10^{-12} . The dipole moment of indene (C_9H_8) of 0.50 D is slightly higher than the dipole moment of propylene (C_3H_6), which has been detected recently in TMC-1, of 0.36 D (51), suggesting that an astronomical detection of indene toward TMC-1 is challenging, but technologically feasible in the context of a high-spectral resolution, high-sensitivity survey using, e.g., the Robert C. Byrd 100 m Green Bank Telescope (GBT) or the Atacama Large Millimeter/submillimeter Array (ALMA). Cyanoindene isomers ($\text{C}_9\text{H}_7\text{CN}$; fig. S5), which may form via rapid, barrierless neutral-neutral reactions of indene with the cyano radical (CN) (52), hold significantly higher dipole moments between 4.03 and 5.70 D, thus classifying “cyano-tagged” indene viable candidates to be searched for. This strategy has been exploited successfully by Chin *et al.* (53) and Lovas *et al.* (54) along with McGuire *et al.* (55) to detect cyanoallene [$\text{H}_2\text{CCCH}(\text{CN})$] and cyanobenzene ($\text{C}_6\text{H}_5\text{CN}$) formed via bimolecular gas-phase reactions of CNs with microwave inactive allene (H_2CCCH_2) (56) and benzene (C_6H_6) (57), respectively. Our astrochemical models predict cyanoindene isomers to be present with fractional abundances of up to 10^{-11} with respect to molecular hydrogen—levels that are comfortably in the realm of the GBT or ALMA—with the larger value of ζ revealing an even stronger effect on the abundances of cyanoindene compared to indene.

DISCUSSION AND CONCLUSIONS

Our combined crossed molecular beams, electronic structure, and astrochemical modeling study reveals that indene may form not only in hot circumstellar envelopes of carbon-rich stars together with planetary nebulae as thought previously but also in cold molecular clouds via facile, barrierless reactions involving the simplest organic radical (methylidyne) with styrene. Because indene carries a five-membered ring, the low-temperature pathway may deliver a population of indene, which could provide a structural motif for the generation of nonplanar PAHs such as corannulene and even fullerenes (Fig. 1). These five-membered rings are critical to bent PAHs out of plane; as evident from kinetic Monte Carlo models of graphene-edge growth, the exclusion of reactions creating five-membered rings from the simulation leads only to planar PAHs (23, 58). It is worth mentioning that PAH formation might also involve nucleation, where reactive surfaces provided by seed particles such as silicon carbides initiate grain growth processes through deposition of aromatic molecules. After ejection to the interstellar medium, the upper layers of these grains, which may contain aromatic molecules, might be desorbed by UV radiation, sputtering, or shuttering by grain-grain collision (59). Furthermore, in solar nebula, the abstraction of a hydrogen atom followed by the addition of acetylene molecules may form significant quantities of PAHs by considering the higher initial concentration based on the astronomical observational results; these processes involve entrance barriers and only operate at elevated temperatures of typically 1000 K and beyond (60). Thus, the present investigation of barrierless, low-temperature pathways to indene may bring us

closer to unraveling the paradox of the injection and destruction time scales of aromatics.

The work reported here represents an important step toward a systematic understanding of the fundamental chemical processes leading to the formation of indene and nonplanar PAHs in low-temperature environments in deep space. Whereas indene has been shown to be the product in high-temperature processes involving reactions of phenyl radicals (C_6H_5) with allene (H_2CCCH_2) and methylacetylene (CH_3CCH) (61, 62) along with the benzyl radical (C_7H_7)–acetylene (C_2H_2) system (63), the MACA mechanism operates at low temperatures such as in molecular clouds. The only other barrierless reaction, which has been recently shown to form indene, is *o*-benzynes (C_6H_4) plus allyl (C_3H_5) (64), but it involves two unstable species not detected in deep space. MACA has the potential to convert any vinyl group (C_2H_3) linked to an aromatic, six-membered ring eventually to a cyclopentadiene moiety via reaction of a methylidyne radical (Fig. 6). MACA can compete with the ethynyl addition mechanism (EAM) (65, 66), which is predicted to convert the vinyl group attached to a PAH molecule to a six-membered ring. Whereas the carbon backbone of the benzene ring stays intact as long as the methylidyne radical adds to the vinyl moiety (Fig. 7), an addition to the benzene ring leads to a complete structural reorganization of the benzene moiety, leading to a newly formed six-membered ring incorporating the vinyl functional group. The complete reorganization of the carbon skeleton of a “stable” aromatic system even at temperatures as low as 10 K leads to a complete “loss of memory” of the molecular structure and is rather unprecedented, as traditional molecular mass growth processes to aromatic systems merely “add” rings to an existing aromatic structure. Considering the crucial role of nonplanar PAHs in the formation of fullerenes and carbonaceous dust particles—commonly referred to as interstellar grains—and in the chemical evolution of the universe, with grains acting as vital molecular factories to synthesize biorelevant organics like amino acids and sugars, the elucidation of the elementary steps leading to dust particles in our galaxy is fundamental to enhance our knowledge of the chemistry of carbonaceous matter in our galaxy.

MATERIALS AND METHODS

Crossed molecular beam experiments

The reaction of the methylidyne (CH ; $X^2\Pi$) radical with styrene (C_8H_8 ; X^1A') was performed in gas phase under single collision conditions exploiting a crossed molecular beam machine (67). A pulsed supersonic beam of methylidyne radicals was produced by photodissociation of helium (99.9999%; Air Gas)–seeded bromoform (CHBr_3 , $\geq 99\%$; Aldrich Chemistry) held in a stainless steel bubbler at a stagnation pressure of 2.2 atm and 283 K. This mixture was introduced into a pulsed piezoelectric valve operating at a repetition rate of 60 Hz, pulse widths of 80 μs , and a peak voltage of -400 V . The 248-nm output of excimer laser (30 Hz; COMPex 110, Coherent Inc.) intersected molecular beam 1 mm downstream of the nozzle (68). A chopper wheel rotating at 120 Hz selected a section of the pulse defined by a peak velocity of $1850 \pm 11 \text{ ms}^{-1}$ and speed ratio of 11.7 ± 0.7 . The rotational temperature was characterized by laser-induced fluorescence to be $14 \pm 1 \text{ K}$ (69). This segment crossed a pulsed supersonic beam of styrene (C_8H_8 , $>99.0\%$; TCI America) seeded in xenon (99.9999%; Matheson) at a fraction of 1% at 550 torr perpendicularly. The section of the supersonic styrene beam crossing the methylidyne radical beam has a peak velocity and speed ratio of

$386 \pm 4 \text{ ms}^{-1}$ and 28.0 ± 0.4 , respectively, resulting in a collision energy of $20.6 \pm 0.2 \text{ kJ mol}^{-1}$ and CM angle $59.1 \pm 0.3^\circ$. The beam characteristics are defined in table S1. The reactive-scattering products were ionized by an electron-impact ionizer operating at 80 eV and 2-mA emission current, before they entered a quadrupole mass spectrometer (QMS, Extrel 150-QC) operating in the TOF mode (70, 71). The designated ion species filtered by the QMS at a specific m/z traveled toward a stainless steel target coated with a thin layer of aluminum biased at -22.5 kV , and a cascade-of-electron pulse was initiated upon impact. The electrons were then expelled from the stainless steel target and flew toward an organic scintillator to generate a photon pulse, before being detected by a Burle photomultiplier tube (model 8850) operating at -1.35 kV . The signal was filtered by a discriminator (Advanced Research Instruments, model F-100TD) at a level of 1.6 mV and fed into a Stanford Research System SR430 multichannel scaler. The rotatable detector allows the collection of angular resolved TOF spectra at discrete angles, integrate and normalize them with respect to the intensity at the CM angle, and then derive the product LAD at a specific m/z . To obtain information on the reaction dynamics, we used a forward-convolution routine to convert the data from the laboratory frame into the CM reference frame (29, 30). Considering the barrierless reaction, the collision energy (E_c) dependence of the cross-section σ was obtained from the line-of-center model as $\sigma \sim E_c^{-1/3}$ (32). The flux contour map, $I(\theta, u) = P(u) \times T(\theta)$, which presents the flux of the reactively scattered products as a function of the CM scattering angle (θ) and product velocity (u), contains all information of the reactive scattering process.

Electronic structure and RRKM calculations

Geometries of the reactants, products, intermediates, and transition states involved in the methylidyne-styrene reaction on the C_9H_9 potential energy surface were optimized at the B3LYP/6-311G(d,p) level of theory (72, 73) with vibrational frequencies computed using the same method. Single-point energies were further improved using the composite G3(MP2,CC) model chemistry scheme (74–76). The G3(MP2,CC)//B3LYP theoretical approach is capable of providing the energetic parameters with “chemical accuracy” within 3 to 6 kJ mol^{-1} for hydrocarbons in terms of average absolute deviations. The Gaussian 09 (77) and MOLPRO 2010 (78) program packages were used for the ab initio calculations. RRKM theory (79–82) was used to compute energy-dependent rate constants of all unimolecular reaction steps on the C_9H_9 surface following the initial addition of the methylidyne radical to styrene and to obtain product branching ratios under single-collision conditions using our in-house UNIMOL code (83).

VRC-TST calculations of rate constants for methylidyne addition to C_6H_6 and C_2H_4

Rate constants for the barrierless CH + benzene and CH + ethylene addition reactions were computed using VRC-TST (84–86). A multifaceted spherical dividing surface (84) used in the calculations was built as the equidistant surface between the pivot points assigned to the associating/dissociating fragments. At short-range distances (less than 5 Å), the pivot point placement was varied along the symmetry axis of the π orbitals of benzene/ethylene. The centers of mass of the reacting fragments served as the pivot points at long-range distances (84). A complex of interacting fragments on a dividing surface was generated using the geometries of CH and benzene/ethylene optimized as separate fragments at the B3LYP/6-311G(d,p) (72, 73)

level of theory. The notation “rigid” is used here to denote the lack of geometrical relaxation in a complex on a dividing surface. The single-point energies of rigid structures were probed at the CCSD(T)/cc-pVDZ (87) level of theory. The single-point energies of the rigid structures were further amended with the one-dimensional geometry relaxation correction (84) and the complete basis set (CBS) correction (88). The one-dimensional geometry relaxation correction was calculated for the minimum energy path (MEP) rigid structures relaxed using B3LYP/6-311G(d,p) geometry optimization. The CBS correction was calculated using the CCSD(T)/cc-pVnZ ($n = D, T, Q$) energies of the rigid MEP structures. To summarize, in the VRC-TST reactive flux calculations, the energies of the rigid structures sampled on a dividing surface were first probed at the CCSD(T)/cc-pVDZ level of theory followed by the ad hoc one-dimensional relaxation and CBS corrections

$$E = E_{\text{rigid}}[\text{CCSD(T)/cc-pVDZ}] + \Delta E[\text{geom}] + \Delta E[\text{CBS}]$$

where E_{rigid} is the single-point energy of the interacting rigid fragments and $\Delta E[\text{geom}]$ is the geometry relaxation correction computed as the difference of CCSD(T)/cc-pVDZ energy of the optimized MEP structure corresponding to a particular value of the R_{CC} distance and the rigid structure at the same R . $\Delta E[\text{CBS}]$ was calculated as follows

$$\Delta E[\text{pVTZ}] = E_{\text{rigid}}[\text{CCSD(T)/cc-VTZ}] - E_{\text{rigid}}[\text{CCSD(T)/cc-VDZ}]$$

$$\Delta E[\text{pVQZ}] = E_{\text{rigid}}[\text{CCSD(T)/cc-VQZ}] - E_{\text{rigid}}[\text{CCSD(T)/cc-VTZ}]$$

$$\Delta E[\text{CBS}] = \Delta E[\text{pVQZ}] + 0.69377 \times (\Delta E[\text{pVQZ}] - \Delta E[\text{pVTZ}])$$

The temperature-dependent high-pressure limit rate constants for the CH + benzene and CH + ethylene addition reactions are shown in fig. S4, and the computed ratios of these rate constants at different temperatures are presented in table S3.

Astrochemical modeling

For this work, the three-phase astrochemical code, Nautilus v1.1, was used (48). In addition to running models using the standard cosmic ray ionization rate of $\zeta = 1.3 \times 10^{-17} \text{ s}^{-1}$, we carried out additional simulations with a value of $\zeta = 1.3 \times 10^{-16} \text{ s}^{-1}$. This latter value is based on the recent study by Ivlev and coworkers (50) of gas and dust temperatures toward L1544, which is another source in Taurus fairly close to TMC-1. It has previously been suggested in a number of recent works that the cosmic ray ionization is higher than the standard value toward the Galactic Center (89–91); however, the study by Ivlev and coworkers is remarkable, in part, because it similarly suggests that the standard value is too low even for regions outside the Galactic Center. To account for cosmic ray-driven reactions, the method of Shingledecker and Herbst (92) and Shingledecker *et al.* (93) is exploited. The physical conditions and elemental abundances appropriate for TMC-1 are listed in tables S5 and S6; an initial carbon-to-oxygen ratio of 1.2 was used (49). Our chemical network is based on that used by Shingledecker *et al.* (94). To it, we added reactions related to the formation of indene (C_9H_8) and similar polycyclic species. New gas-phase reactions are given in table S7, with rates taken from the literature where available or computed via Eqs. 2 and 3; ζ is the cosmic ray ionization rate, and

α describes the efficiency of photodissociation by internally generated UV photons.

$$k_3 = \alpha \left(\frac{T}{300 \text{ K}} \right)^\beta e^{-\frac{\gamma}{T}} \quad (1)$$

$$k_2 = \alpha \zeta \quad (2)$$

To objectively explore the effects of the formation of indene on the icy grains followed by desorption into the gas phase, we also explored (i) neutral-neutral reactions between ground-state species, (ii) the cosmic ray-driven radiolysis of the new species, and (iii) reactions involving one ground-state species and one suprathermal species in a higher electronic state. Suprathermal reactions occur quickly (95, 96), with rate coefficients incorporated based on the attempt frequency (94). Whenever experimental production rates in the ices were not available, we computed the rate coefficients using expression (3) where α is the branching fraction and γ is the G value of formation, which gives the number of molecules produced per 100 eV deposited in the system.

$$k_{\text{rad}} = \alpha \left(\frac{S_e}{100 \text{ eV}} \right) \gamma \left(\phi \frac{\zeta}{10^{-17} \text{ s}^{-1}} \right) \quad (3)$$

Although we have included this grain-surface analog system of the MACA route in our network, its contribution to the overall abundance of gas-phase indene was found to be negligible at levels of less than 1%. The main destruction routes for indene include reactions with carbon atoms at model times less than ca. 10^5 years, and with CNs thereafter. Depletion onto the 10 K grains represents another destruction mechanism for gas-phase indene and the dominant destruction route for cyanoindenes.

SUPPLEMENTARY MATERIALS

Supplementary material for this article is available at <http://advances.sciencemag.org/cgi/content/full/7/1/eabd4044/DC1>

REFERENCES AND NOTES

- A. Leger, J. L. Puget, Identification of the 'unidentified' IR emission features of interstellar dust? *Astron. Astrophys.* **137**, L5–L8 (1984).
- C. Boersma, J. Bregman, L. J. Allamandola, The charge state of polycyclic aromatic hydrocarbons across a reflection nebula, an H_{II} region, and a planetary nebula. *Astrophys. J.* **858**, 67 (2018).
- M. G. Rawlings, A. J. Adamson, C. C. M. Marshall, P. J. Sarre, Near-infrared diffuse interstellar bands towards Her 36. *Mon. Not. R. Astron. Soc.* **485**, 3398–3401 (2019).
- R. Ruiterkamp, T. Halasinski, F. Salama, B. H. Foing, L. J. Allamandola, W. Schmidt, P. Ehrenfreund, Spectroscopy of large PAHs. Laboratory studies and comparison to the diffuse interstellar bands. *Astron. Astrophys.* **390**, 1153–1170 (2002).
- M. Tsuge, C.-Y. Tseng, Y.-P. Lee, Spectroscopy of prospective interstellar ions and radicals isolated in para-hydrogen matrices. *Phys. Chem. Chem. Phys.* **20**, 5344–5358 (2018).
- N. L. J. Cox, J. Cami, A. Farhang, J. Smoker, A. Monreal-Ibero, R. Lallement, P. J. Sarre, C. C. M. Marshall, K. T. Smith, C. J. Evans, P. Royer, H. Linnartz, M. A. Cordiner, C. Joblin, J. T. van Loon, B. H. Foing, N. H. Bhatt, E. Bron, M. Elyajouri, A. de Koter, P. Ehrenfreund, A. Javadi, L. Kaper, H. G. Khosroshadi, M. Laverick, F. Le Petit, G. Mulas, E. Roueff, F. Salama, M. Spaans, The ESO Diffuse Interstellar Bands Large Exploration Survey: EDIBLES I. Project description, survey sample and quality assessment. *Astron. Astrophys.* **606**, A76 (2017).
- R. Ruiterkamp, N. L. J. Cox, M. Spaans, L. Kaper, B. H. Foing, F. Salama, P. Ehrenfreund, PAH charge state distribution and DIB carriers: Implications from the line of sight toward HD 147889. *Astron. Astrophys.* **432**, 515–529 (2005).
- N. L. J. Cox, J. Cami, L. Kaper, P. Ehrenfreund, B. H. Foing, B. B. Ochsendorf, S. H. M. van Hooff, F. Salama, VLT/X-Shooter survey of near-infrared diffuse interstellar bands. *Astron. Astrophys.* **569**, A117 (2014).
- M. Tsuge, M. Bahou, Y.-J. Wu, L. Allamandola, Y.-P. Lee, The infrared spectrum of protonated ovalene in solid para-hydrogen and its possible contribution to interstellar unidentified infrared emission. *Astrophys. J.* **825**, 96 (2016).
- H.-S. Kim, D. R. Wagner, R. J. Saykally, Single photon infrared emission spectroscopy of the gas phase pyrene cation: Support for a polycyclic aromatic hydrocarbon origin of the unidentified infrared emission bands. *Phys. Rev. Lett.* **86**, 5691–5694 (2001).
- A. G. G. M. Tielens, The molecular universe. *Rev. Mod. Phys.* **85**, 1021–1081 (2013).
- W. W. Duley, Polycyclic aromatic hydrocarbons, carbon nanoparticles and the diffuse interstellar bands. *Faraday Discuss.* **133**, 415–425 (2006).
- R. Zenobi, J.-M. Philippoz, R. N. Zare, P. R. Buseck, Spatially resolved organic analysis of the allende meteorite. *Science* **246**, 1026–1029 (1989).
- Y. Wang, Y. Huang, C. M. O. D. Alexander, M. Fogel, G. Cody, Molecular and compound-specific hydrogen isotope analyses of insoluble organic matter from different carbonaceous chondrite groups. *Geochim. Cosmochim. Acta* **69**, 3711–3721 (2005).
- A. G. G. M. Tielens, Interstellar polycyclic aromatic hydrocarbon molecules. *Annu. Rev. Astron. Astrophys.* **46**, 289–337 (2008).
- M. Frenklach, Reaction mechanism of soot formation in flames. *Phys. Chem. Chem. Phys.* **4**, 2028–2037 (2002).
- E. R. Micelotta, A. P. Jones, A. G. G. M. Tielens, Polycyclic aromatic hydrocarbon processing in a hot gas. *Astron. Astrophys.* **510**, A37 (2010).
- E. R. Micelotta, A. P. Jones, A. G. G. M. Tielens, Polycyclic aromatic hydrocarbon processing in interstellar shocks. *Astron. Astrophys.* **510**, A36 (2010).
- I. Cherchneff, The formation of polycyclic aromatic hydrocarbons in evolved circumstellar environments. *EAS Publ. Ser.* **46**, 177–189 (2011).
- M. Frenklach, E. D. Feigelson, Formation of polycyclic aromatic hydrocarbons in circumstellar envelopes. *Astrophys. J.* **341**, 372–384 (1989).
- I. Cherchneff, J. R. Barker, A. G. G. M. Tielens, Polycyclic aromatic hydrocarbon formation in carbon-rich stellar envelopes. *Astrophys. J.* **401**, 269–287 (1992).
- M. Cohen, A. G. G. M. Tielens, J. D. Bregman, Mid-infrared spectra of WC 9 stars: The composition of circumstellar and interstellar dust. *Astrophys. J. Lett.* **344**, L13–L16 (1989).
- R. M. Mahfouz, M. Sauer, S. T. Atwa, R. I. Kaiser, K. Roessler, Interaction of MeV ions and VUV photons with polymers and high molecular hydrocarbons. *Nucl. Instrum. Methods Phys. Res. B* **65**, 447–451 (1992).
- A. Chuvilin, U. Kaiser, E. Bichoutskaia, N. A. Besley, A. N. Khlobystov, Direct transformation of graphene to fullerene. *Nat. Chem.* **2**, 450–453 (2010).
- O. Berné, A. G. G. M. Tielens, Formation of buckminsterfullerene (C_{60}) in interstellar space. *Proc. Natl. Acad. Sci. U.S.A.* **109**, 401–406 (2012).
- L. G. Marin, S. Bejaoui, M. Haggmark, N. Svadlenak, M. de Vries, E. Sciamma-O'Brien, F. Salama, Low-temperature formation of carbonaceous dust grains from PAHs. *Astrophys. J.* **889**, 101 (2020).
- J. A. Miller, M. J. Pilling, J. Troe, Unravelling combustion mechanisms through a quantitative understanding of elementary reactions. *Proc. Combust. Inst.* **30**, 43–88 (2005).
- B. D. Adamson, S. A. Skeen, M. Ahmed, N. Hansen, Detection of aliphatically bridged multi-core polycyclic aromatic hydrocarbons in sooting flames with atmospheric-sampling high-resolution tandem mass spectrometry. *J. Phys. Chem. A* **122**, 9338–9349 (2018).
- X. Gu, Y. Guo, F. Zhang, A. M. Mebel, R. I. Kaiser, Reaction dynamics of carbon-bearing radicals in circumstellar envelopes of carbon stars. *Faraday Discuss.* **133**, 245–275 (2006).
- R. I. Kaiser, C. Ochsenfeld, D. Stranges, M. Head-Gordon, Y. T. Lee, Combined crossed molecular beams and ab initio investigation of the formation of carbon-bearing molecules in the interstellar medium via neutral-neutral reactions. *Faraday Discuss.* **109**, 183–204 (1998).
- M. V. Roux, M. Temprado, J. S. Chickos, Y. Nagano, Critically evaluated thermochemical properties of polycyclic aromatic hydrocarbons. *J. Phys. Chem. Ref. Data* **37**, 1855–1996 (2008).
- R. D. Levine, *Molecular Reaction Dynamics* (Cambridge Univ. Press, 2005).
- W. B. Miller, S. A. Safronan, D. R. Herschbach, Exchange reactions of alkali atoms with alkali halides: A collision complex mechanism. *Discuss. Faraday Soc.* **44**, 108–122 (1967).
- F. Zhang, P. Maksyutenko, R. I. Kaiser, Chemical dynamics of the $\text{CH}(X^2\Pi) + \text{C}_2\text{H}_4(X^1A_{1g})$, $\text{CH}(X^2\Pi) + \text{C}_2\text{D}_4(X^1A_{1g})$, and $\text{CD}(X^2\Pi) + \text{C}_2\text{H}_4(X^1A_{1g})$ reactions studied under single collision conditions. *Phys. Chem. Chem. Phys.* **14**, 529–537 (2012).
- C. He, A. M. Thomas, G. R. Galimova, A. N. Morozov, A. M. Mebel, R. I. Kaiser, Gas-phase formation of fulvenallene (C_7H_6) via the Jahn–Teller distorted tropyli (C_7H_7) radical intermediate under single-collision conditions. *J. Am. Chem. Soc.* **142**, 3205–3213 (2020).
- A. Canosa, I. R. Sims, D. Travers, I. W. M. Smith, B. R. Rowe, Reactions of the methylidene radical with CH_4 , C_2H_2 , C_2H_4 , C_2H_6 , and but-1-ene studied between 23 and 295 K with a CRESU apparatus. *Astron. Astrophys.* **323**, 644–651 (1997).

37. J.-C. Loison, A. Bergeat, Rate constants and the H atom branching ratio of the reactions of the methylidyne $\text{CH}(\text{X}^2\Pi)$ radical with C_2H_2 , C_2H_4 , C_3H_4 (methylacetylene and allene), C_3H_6 (propene) and C_4H_8 (*trans*-butene). *Phys. Chem. Chem. Phys.* **11**, 655–664 (2009).
38. H. Thiesemann, E. P. Clifford, C. A. Taatjes, S. J. Klippenstein, Temperature dependence and deuterium kinetic isotope effects in the $\text{CH}(\text{CD}) + \text{C}_3\text{H}_4$ (C_2D_4) reaction between 295 and 726 K. *J. Phys. Chem. A* **105**, 5393–5401 (2001).
39. S. Hamon, S. D. Le Picard, A. Canosa, B. R. Rowe, I. W. M. Smith, Low temperature measurements of the rate of association to benzene dimers in helium. *J. Chem. Phys.* **112**, 4506–4516 (2000).
40. M. R. Berman, J. W. Fleming, A. B. Harvey, M. C. Lin, Temperature dependence of the reactions of CH radicals with unsaturated hydrocarbons. *Chem. Phys.* **73**, 27–33 (1982).
41. M. D. Lodriguito, G. Lendvay, G. C. Schatz, Trajectory surface-hopping study of methane photodissociation dynamics. *J. Chem. Phys.* **131**, 224320 (2009).
42. M. Gerin, D. A. Neufeld, J. R. Goicoechea, Interstellar hydrides. *Annu. Rev. Astron. Astrophys.* **54**, 181–225 (2016).
43. D. Belisario-Lara, A. M. Mebel, R. I. Kaiser, Computational study on the unimolecular decomposition of JP-8 Jet fuel surrogates III: Butylbenzene isomers (*n*-, *s*-, and *t*- $\text{C}_{14}\text{H}_{10}$). *J. Phys. Chem. A* **122**, 3980–4001 (2018).
44. M. J. Abplanalp, R. I. Kaiser, Implications for extraterrestrial hydrocarbon chemistry: Analysis of acetylene (C_2H_2) and D2-acetylene (C_2D_2) ices exposed to ionizing radiation via ultraviolet-visible spectroscopy, infrared spectroscopy, and reflection time-of-flight mass spectrometry. *Astrophys. J.* **889**, 3 (2020).
45. J. D. Thrower, A. G. M. Abdulgaliil, M. P. Collings, M. R. S. McCoustra, D. J. Burke, W. A. Brown, A. Dawes, P. J. Holtom, P. Kendall, N. J. Mason, F. Jamme, H. J. Fraser, F. J. M. Rutten, Photon- and electron-stimulated desorption from laboratory models of interstellar ice grains. *J. Vac. Sci. Technol. A* **28**, 799–806 (2010).
46. B. B. Dangi, D. S. N. Parker, R. I. Kaiser, A. Jamal, A. M. Mebel, A combined experimental and theoretical study on the gas-phase synthesis of toluene under single collision conditions. *Angew. Chem. Int. Ed.* **52**, 7186–7189 (2013).
47. A. M. Thomas, C. He, L. Zhao, G. R. Galimova, A. M. Mebel, R. I. Kaiser, A combined experimental and computational study on the reaction dynamics of the 1-Propynyl (CH_3CC) – 1,3-butadiene ($\text{CH}_2\text{CHCHCH}_2$) system and the formation of toluene under single collision conditions. *J. Phys. Chem. A* **123**, 4104–4118 (2019).
48. M. Ruaud, V. Wakelam, F. Hersant, Gas and grain chemical composition in cold cores as predicted by the Nautilus three-phase model. *Mon. Not. R. Astron. Soc.* **459**, 3756–3767 (2016).
49. U. Hincelin, V. Wakelam, F. Hersant, S. Guilloteau, J.-C. Loison, P. Honvault, J. Troe, Oxygen depletion in dense molecular clouds: A clue to a low O_2 abundance? *Astron. Astrophys.* **530**, A61 (2011).
50. A. V. Ivlev, K. Silsbee, O. Sipilä, P. Caselli, Gas and dust temperature in prestellar cores revisited: New limits on cosmic-ray ionization rate. *Astrophys. J.* **884**, 176 (2019).
51. N. Marinello, J. Cernicharo, M. Agúndez, E. Roueff, M. Gerin, J. Martín-Pintado, Discovery of interstellar propylene (CH_2CHCH_3): Missing links in interstellar gas-phase chemistry. *Astrophys. J.* **665**, L127–L130 (2007).
52. R. I. Kaiser, N. Balucani, The formation of nitriles in hydrocarbon-rich atmospheres of planets and their satellites: Laboratory investigations by the crossed molecular beam technique. *Acc. Chem. Res.* **34**, 699–706 (2001).
53. Y.-N. Chin, R. I. Kaiser, C. Lemme, C. Henkel, Detection of interstellar cyanoallene and its implications for astrochemistry. *AIP Conf. Proc.* **855**, 149–153 (2006).
54. F. J. Lovas, A. J. Remijan, J. M. Hollis, P. R. Jewell, L. E. Snyder, Hyperfine structure identification of interstellar cyanoallene toward TMC-1. *Astrophys. J. Lett.* **637**, L37–L40 (2006).
55. B. A. McGuire, A. M. Burkhardt, S. Kalenskii, C. N. Shingledecker, A. J. Remijan, E. Herbst, M. C. McCarthy, Detection of the aromatic molecule benzonitrile (*c*- $\text{C}_6\text{H}_5\text{CN}$) in the interstellar medium. *Science* **359**, 202–205 (2018).
56. L. C. L. Huang, N. Balucani, Y. T. Lee, R. I. Kaiser, Y. Osamura, Crossed beam reaction of the cyano radical, $\text{CN}(\text{X}^2\Sigma^+)$, with methylacetylene, $\text{H}_3\text{CCH}(\text{X}^1\text{A}_1)$: Observation of cyanopropyne, $\text{CH}_3\text{CCCN}(\text{X}^1\text{A}_1)$, and cyanoallene, $\text{H}_2\text{CCCHCN}(\text{X}^1\text{A}')$. *J. Chem. Phys.* **111**, 2857–2860 (1999).
57. N. Balucani, O. Asvany, A. H. H. Chang, S. H. Lin, Y. T. Lee, R. I. Kaiser, H. F. Bettinger, P. v. R. Schleyer, H. F. Schaefer III, Crossed beam reaction of cyano radicals with hydrocarbon molecules. I. Chemical dynamics of cyanobenzene ($\text{C}_6\text{H}_5\text{CN}$; X^1A_1) and perdeutero cyanobenzene ($\text{C}_6\text{D}_5\text{CN}$; X^1A_1) formation from reaction of $\text{CN}(\text{X}^2\Sigma^+)$ with benzene $\text{C}_6\text{H}_6(\text{X}^1\text{A}_{1g})$, and *d*₆-benzene $\text{C}_6\text{D}_6(\text{X}^1\text{A}_{1g})$. *J. Chem. Phys.* **111**, 7457–7471 (1999).
58. R. Whitesides, M. Frenklach, Detailed kinetic Monte Carlo simulations of graphene-edge growth. *J. Phys. Chem. A* **114**, 689–703 (2010).
59. B. J. Cadwell, H. Wang, E. D. Feigelson, M. Frenklach, Induced nucleation of carbon dust in red giant stars. *Astrophys. J.* **429**, 285–299 (1994).
60. W. A. Morgan Jr., E. D. Feigelson, H. Wang, M. Frenklach, A new mechanism for the formation of meteoritic kerogen-like material. *Science* **252**, 109–112 (1991).
61. D. S. N. Parker, F. Zhang, R. I. Kaiser, V. V. Kislov, A. M. Mebel, Indene formation under single-collision conditions from the reaction of phenyl radicals with allene and methylacetylene—A crossed molecular beam and ab initio study. *Chem. Asian J.* **6**, 3035–3047 (2011).
62. F. Zhang, R. I. Kaiser, V. V. Kislov, A. M. Mebel, A. Golan, M. Ahmed, A VUV photoionization study of the formation of the indene molecule and its isomers. *J. Phys. Chem. Lett.* **2**, 1731–1735 (2011).
63. D. S. N. Parker, R. I. Kaiser, O. Kostko, M. Ahmed, Selective formation of indene through the reaction of benzyl radicals with acetylene. *ChemPhysChem* **16**, 2091–2093 (2015).
64. M. N. McCabe, P. Hemberger, E. Reusch, A. Bodi, J. Bouwman, Off the beaten path: Almost clean formation of indene from the ortho-benzyne + allyl reaction. *J. Phys. Chem. Lett.* **11**, 2859–2863 (2020).
65. A. M. Mebel, V. V. Kislov, R. I. Kaiser, Photoinduced mechanism of formation and growth of polycyclic aromatic hydrocarbons in low-temperature environments via successive ethynyl radical additions. *J. Am. Chem. Soc.* **130**, 13618–13629 (2008).
66. A. Landera, R. I. Kaiser, A. M. Mebel, Addition of one and two units of C_2H to styrene: A theoretical study of the C_{10}H_9 and C_{12}H_9 systems and implications towards growth of polycyclic aromatic hydrocarbons at low temperatures. *J. Chem. Phys.* **134**, 024302 (2011).
67. R. I. Kaiser, P. Maksyutenko, C. Ennis, F. Zhang, X. Gu, S. P. Krishtal, A. M. Mebel, O. Kostko, M. Ahmed, Untangling the chemical evolution of Titan's atmosphere and surface—from homogeneous to heterogeneous chemistry. *Faraday Discuss.* **147**, 429–478 (2010).
68. A. M. Thomas, L. Zhao, C. He, G. R. Galimova, A. M. Mebel, R. I. Kaiser, Directed gas-phase synthesis of triafulvene under single-collision conditions. *Angew. Chem. Int. Ed.* **58**, 15488–15495 (2019).
69. P. Maksyutenko, F. Zhang, X. Gu, R. I. Kaiser, A crossed molecular beam study on the reaction of methylidyne radicals [$\text{CH}(\text{X}^2\Pi)$] with acetylene [$\text{C}_2\text{H}_2(\text{X}^1\Sigma_g^+)$]-competing $\text{C}_3\text{H}_2 + \text{H}$ and $\text{C}_3\text{H} + \text{H}_2$ channels. *Phys. Chem. Chem. Phys.* **13**, 240–252 (2011).
70. G. O. Brink, Electron bombardment molecular beam detector. *Rev. Sci. Instrum.* **37**, 857–860 (1966).
71. N. R. Daly, Scintillation type mass spectrometer ion detector. *Rev. Sci. Instrum.* **31**, 264–267 (1960).
72. A. D. Becke, Density-functional thermochemistry. III. The role of exact exchange. *J. Chem. Phys.* **98**, 5648–5652 (1993).
73. C. Lee, W. Yang, R. G. Parr, Development of the Colic-Salvetti correlation-energy formula into a functional of the electron density. *Phys. Rev. B* **37**, 785–789 (1988).
74. L. A. Curtiss, K. Raghavachari, P. C. Redfern, V. Rassolov, J. A. Pople, Gaussian-3 (G3) theory for molecules containing first and second-row atoms. *J. Chem. Phys.* **109**, 7764–7776 (1998).
75. L. A. Curtiss, K. Raghavachari, P. C. Redfern, A. G. Baboul, J. A. Pople, Gaussian-3 theory using coupled cluster energies. *Chem. Phys. Lett.* **314**, 101–107 (1999).
76. A. G. Baboul, L. A. Curtiss, P. C. Redfern, K. Raghavachari, Gaussian-3 theory using density functional geometries and zero-point energies. *J. Chem. Phys.* **110**, 7650–7657 (1999).
77. M. J. Frisch, G. W. Trucks, H. B. Schlegel, G. E. Scuseria, M. A. Robb, J. R. Cheeseman, G. Scalmani, V. Barone, B. Mennucci, G. A. Petersson, *Gaussian 09, Revision A.1* (Gaussian Inc., 2009).
78. H. J. Werner, P. J. Knowles, R. Lindh, F. R. Manby, M. Schütz, P. Celani, T. Korona, G. Rauhut, R. D. Amos, A. Bernhardsson, MOLPRO, version 2010.1, a package of ab initio programs, see <http://www.molpro.net>.
79. P. J. Robinson, K. A. Holbrook, *Unimolecular Reactions* (Wiley, 1972).
80. H. Eyring, S. H. Lin, S. M. Lin, *Basic Chemical Kinetics* (John Wiley and Sons Inc., 1980).
81. J. I. Steinfeld, J. S. Francisco, W. L. Hase, *Chemical Kinetics and Dynamics* (Prentice Hall, 1982).
82. V. V. Kislov, T. L. Nguyen, A. M. Mebel, S. H. Lin, S. C. Smith, Photodissociation of benzene under collision-free conditions: An ab initio/Rice–Ramsperger–Kassel–Marcus study. *J. Chem. Phys.* **120**, 7008–7017 (2004).
83. C. He, L. Zhao, A. M. Thomas, A. N. Morozov, A. M. Mebel, R. I. Kaiser, Elucidating the chemical dynamics of the elementary reactions of the 1-propynyl radical (CH_3CC ; X^2A_1) with Methylacetylene (H_3CCCH ; X^1A_1) and Allene (H_2CCCH_2 ; X^1A_1). *J. Phys. Chem. A* **123**, 5446–5462 (2019).
84. Y. Georgievskii, J. A. Miller, S. J. Klippenstein, Association rate constants for reactions between resonance-stabilized radicals: $\text{C}_3\text{H}_3 + \text{C}_3\text{H}_3$, $\text{C}_3\text{H}_3 + \text{C}_3\text{H}_5$, and $\text{C}_3\text{H}_5 + \text{C}_3\text{H}_5$. *Phys. Chem. Chem. Phys.* **9**, 4259–4268 (2007).
85. S. J. Klippenstein, Variational optimizations in the Rice–Ramsperger–Kassel–Marcus theory calculations for unimolecular dissociations with no reverse barrier. *J. Chem. Phys.* **96**, 367–371 (1992).
86. Y. Georgievskii, S. J. Klippenstein, Variable reaction coordinate transition state theory: Analytic results and application to the $\text{C}_2\text{H}_3 + \text{H} \rightarrow \text{C}_2\text{H}_4$ reaction. *J. Chem. Phys.* **118**, 5442–5455 (2003).
87. T. H. Dunning Jr., Gaussian basis sets for use in correlated molecular calculations. I. The atoms boron through neon and hydrogen. *J. Chem. Phys.* **90**, 1007–1023 (1989).
88. J. M. L. Martin, O. Uzan, Basis set convergence in second-row compounds. The importance of core polarization functions. *Chem. Phys. Lett.* **282**, 16–24 (1998).

89. Y. Ao, C. Henkel, K. M. Menten, M. A. Requena-Torres, T. Stanke, R. Mauersberger, S. Aalto, S. Mühle, J. Mangum, The thermal state of molecular clouds in the Galactic center: Evidence for non-photon-driven heating. *Astron. Astrophys.* **550**, A135 (2013).
90. F. Yusef-Zadeh, W. Cotton, S. Viti, M. Wardle, M. Royster, Widespread methanol emission from the galactic center: The role of cosmic rays. *Astrophys. J. Lett.* **764**, L19 (2013).
91. F. Yusef-Zadeh, J. W. Hewitt, M. Wardle, V. Tatischeff, D. A. Roberts, W. Cotton, H. Uchiyama, M. Nobukawa, T. G. Tsuru, C. Heinke, M. Royster, Interacting cosmic rays with molecular clouds: A bremsstrahlung origin of diffuse high-energy emission from the inner $2^\circ \times 1^\circ$ of the galactic center. *Astrophys. J.* **762**, 33 (2013).
92. C. N. Shingledecker, E. Herbst, A general method for the inclusion of radiation chemistry in astrochemical models. *Phys. Chem. Chem. Phys.* **20**, 5359–5367 (2018).
93. C. N. Shingledecker, G. Molpeceres, V. M. Rivilla, L. Majumdar, J. Kästner, Isomers in interstellar environments. I. The case of Z- and E-cyanomethanimine. *Astrophys. J.* **897**, 158 (2020).
94. C. N. Shingledecker, J. Tennis, R. Le Gal, E. Herbst, On cosmic-ray-driven grain chemistry in cold core models. *Astrophys. J.* **861**, 20 (2018).
95. R. J. Morton, R. Kaiser, Kinetics of suprathreshold hydrogen atom reactions with saturated hydrides in planetary and satellite atmospheres. *Planet. Space Sci.* **51**, 365–373 (2003).
96. R. I. Kaiser, K. Roessler, Theoretical and laboratory studies on the interaction of cosmic-ray particles with interstellar ices. III. Suprathreshold chemistry-induced formation of hydrocarbon molecules in solid methane (CH_4), ethylene (C_2H_4), and acetylene (C_2H_2). *Astrophys. J.* **503**, 959–975 (1998).
97. A. M. Tarr, O. P. Strausz, H. E. Gunning, Reactions of the ethynyl radical part 2.–With alkenes. *Trans. Faraday Soc.* **62**, 1221–1230 (1966).
98. B. Nizamov, S. R. Leone, Kinetics of C_2H reactions with hydrocarbons and nitriles in the 104–296 K temperature range. *J. Phys. Chem. A* **108**, 1746–1752 (2004).
99. B. M. Jones, F. Zhang, R. I. Kaiser, A. Jamal, A. M. Mebel, M. A. Cordiner, S. B. Chamley, Formation of benzene in the interstellar medium. *Proc. Natl. Acad. Sci. U.S.A.* **108**, 452–457 (2011).
100. A. Bergeat, J.-C. Loison, Reaction of carbon atoms, C ($2p^2, ^3P$) with C_2H_2 , C_2H_4 and C_6H_6 : Overall rate constant and relative atomic hydrogen production. *Phys. Chem. Chem. Phys.* **3**, 2038–2042 (2001).
101. I. Hahndorf, Y. T. Lee, R. I. Kaiser, L. Vereecken, J. Peeters, H. F. Bettinger, P. R. Schreiner, P. V. R. Schleyer, W. D. Allen, H. F. Schaefer III, A combined crossed-beam, ab initio, and Rice–Ramsperger–Kassel–Marcus investigation of the reaction of carbon atoms $\text{C}(^3P_j)$ with benzene, $\text{C}_6\text{H}_6(X^1A_{1g})$ and d6-benzene, $\text{C}_6\text{D}_6(X^1A_{1g})$. *J. Chem. Phys.* **116**, 3248–3262 (2002).
102. X. Gu, Y. Guo, F. Zhang, A. M. Mebel, R. I. Kaiser, A crossed molecular beams study of the reaction of dicarbon molecules with benzene. *Chem. Phys. Lett.* **436**, 7–14 (2007).
103. H. Reisler, M. S. Mangir, C. Wittig, Kinetics of free radicals generated by IR laser photolysis. IV. Intersystem crossings and reactions of $\text{C}_2(X^1\Sigma^+_g)$ and $\text{C}_2(a^3\Pi_u)$ in the gaseous phase. *J. Chem. Phys.* **73**, 2280–2286 (1980).
104. I. R. Cooke, D. Gupta, J. P. Messinger, I. R. Sims, Benzonitrile as a proxy for benzene in the cold ISM: Low-temperature rate coefficients for $\text{CN} + \text{C}_6\text{H}_6$. *Astrophys. J. Lett.* **891**, L41 (2020).
105. A. Landera, A. M. Mebel, R. I. Kaiser, Theoretical study of the reaction mechanism of ethynyl radical with benzene and related reactions on the C_6H_7 potential energy surface. *Chem. Phys. Lett.* **459**, 54–59 (2008).
106. F. Goulay, S. R. Leone, Low-temperature rate coefficients for the reaction of ethynyl radical (C_2H) with benzene. *J. Phys. Chem. A* **110**, 1875–1880 (2006).

Acknowledgments: C.N.S. thanks V. Wakelam for the use of the Nautilus-v1.1 code.

Funding: This work was supported by the U.S. Department of Energy, Basic Energy Sciences DE-FG02-03ER15411 (experimental studies, to R.I.K.) and DE-FG02-04ER15570 (computational studies, to A.M.M.) to the University of Hawaii and Florida International University, respectively.

Author contributions: R.I.K. designed research and managed the overall project; S.D., G.R.G., H.W., A.M.T., C.H., Z.Y., A.N.M., C.N.S., A.M.M., and R.I.K. performed research; S.D., G.R.G., H.W., C.N.S., A.M.M., and R.I.K. analyzed data and wrote the paper. **Competing interests:** The authors declare that they have no competing interests. **Data and materials availability:** All data needed to evaluate the conclusions in the paper are present in the paper and/or the Supplementary Materials. Additional data related to this paper may be requested from the authors.

Submitted 18 June 2020

Accepted 4 November 2020

Published 1 January 2021

10.1126/sciadv.abd4044

Citation: S. Doddipatla, G. R. Galimova, H. Wei, A. M. Thomas, C. He, Z. Yang, A. N. Morozov, C. N. Shingledecker, A. M. Mebel, R. I. Kaiser, Low-temperature gas-phase formation of indene in the interstellar medium. *Sci. Adv.* **7**, eabd4044 (2021).

Low-temperature gas-phase formation of indene in the interstellar medium

Srinivas Doddipatla, Galiya R. Galimova, Hongji Wei, Aaron M. Thomas, Chao He, Zhenghai Yang, Alexander N. Morozov, Christopher N. Shingledecker, Alexander M. Mebel and Ralf I. Kaiser

Sci Adv 7 (1), eabd4044.
DOI: 10.1126/sciadv.abd4044

ARTICLE TOOLS	http://advances.sciencemag.org/content/7/1/eabd4044
SUPPLEMENTARY MATERIALS	http://advances.sciencemag.org/content/suppl/2020/12/21/7.1.eabd4044.DC1
REFERENCES	This article cites 100 articles, 5 of which you can access for free http://advances.sciencemag.org/content/7/1/eabd4044#BIBL
PERMISSIONS	http://www.sciencemag.org/help/reprints-and-permissions

Use of this article is subject to the [Terms of Service](#)

Science Advances (ISSN 2375-2548) is published by the American Association for the Advancement of Science, 1200 New York Avenue NW, Washington, DC 20005. The title *Science Advances* is a registered trademark of AAAS.

Copyright © 2021 The Authors, some rights reserved; exclusive licensee American Association for the Advancement of Science. No claim to original U.S. Government Works. Distributed under a Creative Commons Attribution NonCommercial License 4.0 (CC BY-NC).